Solar Energy Materials & Solar Cells 115 (2013) 189–198

Contents lists available at SciVerse ScienceDirect

Solar Energy Materials & Solar Cells

journal homepage: www.elsevier.com/locate/solmat

# Stability of the regeneration of the boron–oxygen complex in silicon solar cells during module integration

Fabian Fertig *, Johannes Greulich, Juliane Broisch, Daniel Biro, Stefan Rein

*Fraunhofer Institute for Solar Energy Systems ISE, Heidenhofstr. 2, D-79110 Freiburg, Germany*

ARTICLE INFO

*Article history:*
Received 20 December 2012
Received in revised form
30 January 2013
Accepted 31 January 2013
Available online 10 May 2013

*Keywords:*
Cz
Boron–oxygen
Module
Degradation
Regeneration

ABSTRACT

Light-induced degradation (LID) in boron-doped *p*-type Czochralski (Cz) silicon is caused by a boron–oxygen (BO) complex, which may be permanently deactivated by simultaneous illumination and heating leading to a permanent regeneration of carrier lifetime and solar cell performance. Up to now, regeneration has only been investigated on wafer and solar cell level. In this work, we investigate whether the regeneration gain on solar cell level can be transferred to module level. For this purpose, we fabricated solar cells with passivated emitter and rear on boron-doped *p*-type Cz and float zone wafers. The cells are extensively characterised regarding losses in cell performance due to LID by preparing different defect states with certain temperature and illumination treatments. The effect of the injection-dependent carrier lifetime caused by the BO complex in its active state on fill factor is investigated in detail theoretically and experimentally, developing a descriptive explanation. Finally, it is shown by integrating solar cells in the degraded and regenerated state into solar modules, that the regeneration effect can be transferred to module level and is stable upon subsequent illumination of the module.



## 1. Introduction

Monocrystalline silicon ingots crystallised via the Czrochalski (Cz) technique [1–3] and doped with boron represent one of the most widely used sources for solar silicon wafers. Since the silicon feedstock is molten in a quartz crucible, oxygen diffuses from the crucible walls into the silicon melt and is incorporated into the silicon crystal [1–3]. Hence, boron and oxygen can form the highly recombination-active boron–oxygen (BO) defect [4,5] in standard industrial Cz *p*-type solar silicon. In its active state, this defect limits the excess carrier lifetime in *p*-type silicon significantly and therefore the maximum conversion efficiency of *p*-type silicon solar cells [6,7]. The characteristics of this defect and its parameterisation have been the subject of intensive research work in the past. This research revealed that the defect is metastable and can be activated upon illumination or carrier injection and fully deactivated upon annealing in the dark [8,9], the transformation between the two defect states being fully reversible.

More recently, Herguth et al. [10] discovered that the BO defect can be permanently deactivated by combined illumination and annealing, which is known as so-called regeneration. The temperatures required for regeneration vary strongly from $T=70$ °C to 215 °C in literature [10,11]. For reported regeneration of solar cells (in contrast to lifetime samples), $T=140$ °C is usually not exceeded. It is known that the regenerated state may be destroyed and the defect reactivated at elevated temperatures above $T=170$ °C in the dark [10] and for some samples (including lifetime samples) after illumination at elevated temperatures for a long time [11,12] while the latter effect is not always observed [12]. However, no information is available on the stability of the regenerated state during thermal processes such as soldering and lamination during module assembly. As temperatures in these process steps may exceed $T=200$ °C significantly [13], they are in the critical range where regeneration may be reversed. Hence, this work aims at investigating if the regenerated state of the boron–oxygen defect which is established on solar cell level is stable upon the subsequent module assembly.

For this purpose, passivated emitter and rear (PERC [14]) solar cells have been processed at Fraunhofer ISE on industrial boron-doped *p*-type Cz silicon wafers. The effect of activation, deactivation and regeneration of the BO defect on solar cell performance is investigated in detail taking into account the impact of changes in the injection-dependence of the minority carrier lifetime upon defect transformation on fill factor. Subsequently, one degraded and one regenerated cell are integrated into single-cell mini-modules to investigate whether the achieved gain on cell level is transferable to module level. Within all steps, a FZ solar cell is used to monitor possible process-induced effects.

## 2. Experimental

To evaluate the stability of the regenerated state of the boron–oxygen complex during module integration, we fabricated

* Corresponding author. Tel.: +49 761 4588 5482.
*E-mail address:* fabian.fertig@ise.fraunhofer.de (F. Fertig).

0927-0248/$ - see front matter © 2013 Elsevier B.V. All rights reserved.
http://dx.doi.org/10.1016/j.solmat.2013.01.047

solar cells on industrial equipment [15]. To increase the sensitivity of solar cell performance on bulk lifetime effects, a PERC process called "thermal oxide passivated all sides" (TOPAS) including a selective emitter has been applied. Screen-printing has been used for metallisation; the front side contact finger pitch is $d_{\mathrm{finger}}=2.2$ mm and the rear side contact spacing has been adapted to base resistivity using an analytical model [16]. Process details can be found in [17,18]. The wafer material used is industrial, boron-doped $p$-type Cz silicon with a base resistivity of $\rho_{\mathrm{b,Cz}}=2.3\,\Omega\,\mathrm{cm}$ and FZ silicon with $\rho_{\mathrm{b,FZ}}=0.5\,\Omega\,\mathrm{cm}$; the format of the wafers is pseudo-square with an edge length of $d_{\mathrm{edge}}=125$ mm and the wafer thickness is $d_{\mathrm{wafer}}=200$ μm before and $d_{\mathrm{cell}}=160$ μm after cell processing. All wafers are processed equally within the same batch. The FZ wafers are used as a reference to monitor possible process-induced effects through the subsequent treatment after cell processing which are not material-related.

Fig. 1 depicts a schematic of the experimental design; two very similar solar cells from Cz wafers (cell A and cell B) and one reference cell from a FZ wafer are (in chronological order) annealed at a temperature of $T=250$ °C for a time of $t=20$ min in the dark resulting in the boron–oxygen defect being completely deactivated, and then degraded for $t\approx 48$ h at an illumination intensity of $E>0.2$ suns ($1\ \mathrm{sun}\triangleq 1\ \mathrm{kW/m^2}$) at $T\leq 40$ °C which fully activates the BO defect. After degradation, Cz cell B and the FZ reference cell are regenerated at $E=1$ sun and $T=140$ °C for $t=2.7$ h. The stability of the regenerated state is tested by illumination at $E>0.2$ suns for $t\approx 5$ days at $T\leq 40$ °C since light-induced re-degradation at room temperature after successful regeneration of BO has been sometimes observed on lifetime samples in literature [11]. The other Cz cell A is neither regenerated nor tested on stability but left in the degraded state.

After preparation of the degraded and the regenerated defect state in cell A and cell B, respectively, all three cells are built into mini-modules and subsequently illuminated at $E>0.2$ suns for $t\approx 48$ h at $T\leq 40$ °C. The module assembly consists of manual contact soldering at $T\approx 245$ °C and a lamination process of the EVA (ethylene-vinyl acetate), front side glass and rear side backsheet. The locally induced temperatures during soldering are comparable to an industrial stringer process where an entire cell is soldered at a temperature of $T\approx 225$ °C within $t=1$–2 s. Before contact soldering, the cells are pre-heated to $T=120$ °C. The temperature profile of the lamination process consists of a ramp-up from $T_{\mathrm{start}}=40$ °C to $T_{\mathrm{plateau}}=133$ °C within $t_{\mathrm{ramp}}=8$ min, a subsequent plateau with $T_{\mathrm{plateau}}=133$ °C for $t_{\mathrm{plateau}}=15.5$ min and a final ramp down to $T_{\mathrm{end}}=40$ °C within $t_{\mathrm{ramp}}=7$ min. During lamination, the cells are in the dark.

In-between each experimental step, all cells respectively modules are characterised by means of $I$–$V$ (current–voltage) and suns–$V_{\mathrm{oc}}$ [19] measurements.

## 3. Effect of the boron–oxygen defect on solar cell performance

The degradation of minority carrier lifetime in the bulk due to activation of the BO complex can degrade all three characteristic illuminated $I$–$V$ parameters: short-circuit current density $J_{\mathrm{sc}}$, open-circuit voltage $V_{\mathrm{oc}}$ and fill factor $FF$. The impact of a strong injection-dependence of the Shockley–Read–Hall lifetime of a defect on fill factor has been shown e.g. by Schmidt et al. [20] for the BO defect using a numerical simulation and by Macdonald and Cuevas [21] using an analytical approach for multicrystalline silicon. In order to understand qualitatively the losses in $V_{\mathrm{oc}}$ and $FF$ induced by the BO defect similar to Macdonald and Cuevas [21], we use a simple zero-dimensional solar cell model (that is the solar cell is considered as a point), which already illustrates the impact of changes in the injection dependence of the carrier lifetime on solar cell performance. The model is not intended as a quantitative description of the three solar cells but shall give a more instructive and descriptive explanation than numerical simulations.

For the correlation of excess carrier density $\Delta n$ and voltage $V$ representing the split of the quasi-Fermi-levels,

$$np=(\Delta n+n_0)(\Delta n+p_0)=n_{\mathrm{i}}^2\exp\left(\frac{V}{V_{\mathrm{t}}}\right)\approx\Delta n(\Delta n+N_{\mathrm{A}}) \tag{1}$$

holds in $p$-type silicon, with $n$ and $p$ being the electron and hole densities, respectively, $n_0$ and $p_0$ the densities in thermal equilibrium, $n_{\mathrm{i}}$ the intrinsic carrier density, $N_{\mathrm{A}}$ the acceptor density and $V_{\mathrm{t}}=kT/q$ the thermal voltage with Boltzmann constant $k$, temperature $T$ and elementary charge $q$. For our approach, we consider recombination via defects according to Shockley–Read–Hall [22,23] (SRH) and Auger recombination using the parameterisation of Kerr and Cuevas [24]. For the effective excess carrier lifetime,

$$\tau_{\mathrm{eff}}=\frac{1}{(1/\tau_{\mathrm{SRH}})+(1/\tau_{\mathrm{Auger}})}=\frac{\Delta n}{R_{\mathrm{SRH}}+R_{\mathrm{Auger}}}=\frac{\Delta n}{R} \tag{2}$$

follows, with recombination rate $R$. In the simple zero-dimensional solar cell model, $\Delta n$ is assumed to be constant across the bulk and all other recombination sources in a solar cell (emitter, space charge region, and surfaces) are neglected. Therefore, the lifetime effects are expected to be more pronounced in the model than in a real device. The correlation between current density $J$ and voltage $V$ can thus be stated as

$$J(V)=\underbrace{WqR(\Delta n(V))}_{J_{\mathrm{rec}}(V)}-J_{\mathrm{ph}}=\underbrace{\frac{Wq}{\tau_{\mathrm{eff}}(\Delta n(V))}\cdot\left(-\frac{N_{\mathrm{A}}}{2}+\sqrt{\frac{N_{\mathrm{A}}^2}{4}+n_{\mathrm{i}}^2\exp\left(\frac{V}{V_{\mathrm{t}}}\right)}\right)}_{J_{\mathrm{rec}}(V)}-J_{\mathrm{ph}}, \tag{3}$$

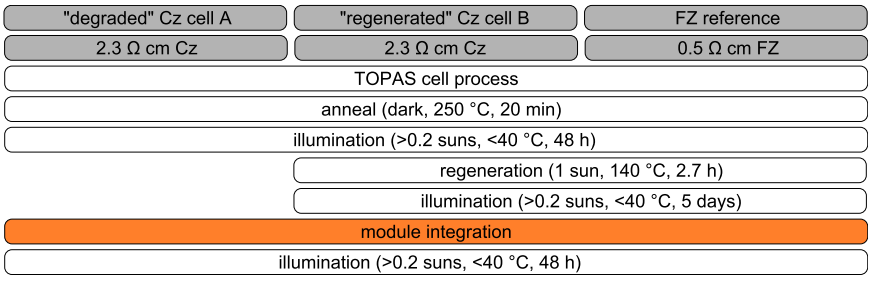


**Fig. 1.** Sketch of the experimental design. Before module assembly, Cz cell A is brought into the degraded state, while Cz cell B and a FZ reference cell are brought into the regenerated state. In-between each step, $I$–$V$ and suns–$V_{\mathrm{oc}}$ measurements are performed.

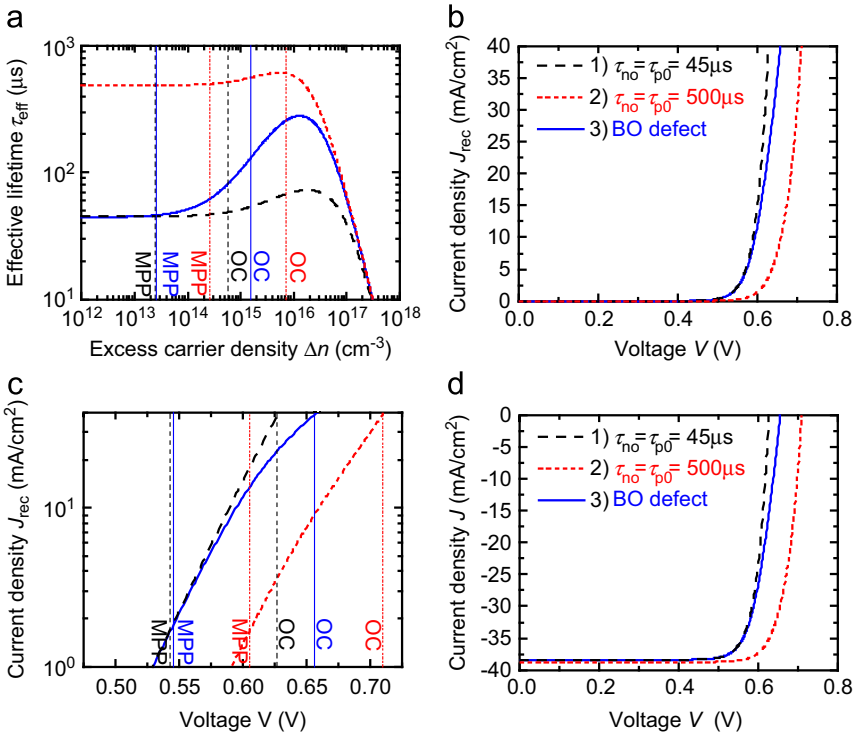


**Fig. 2.** (a) Effective lifetime for SRH defects with (case 1) $E_t=E_i$ and $\tau_{n0}=\tau_{p0}=45$ µs (black dashed line), (case 2) $E_t=E_i$ and $\tau_{n0}=\tau_{p0}=500$ µs (red dotted line) and (case 3) the parameterisation of the BO defect according to [27] with $m=2$, $[B_s]=6.23\times10^{15}$ cm$^{-3}$ and $[O_i]=7.5\times10^{17}$ cm$^{-3}$ based on [25,26] (blue solid line). (b) Resulting $J$–$V$ curves for the lifetimes from (a) with $J_{ph}=0$ mA/cm$^2$, see Eq. (3). (c) Semi-logarithmic display of (b) in the voltage range between MPP and OC. (d) Illuminated $J$–$V$ curves assuming measured $J_{sc}$ values of the annealed state for case 2 and of the degraded state for cases 1 and 3. (For interpretation of the references to colour in this figure legend, the reader is referred to the web version of this article.)

with $W$ being the width of the solar cell, $J_{rec}$ the recombination and $J_{ph}$ the photo-generated current density.

Fig. 2a shows the effective carrier lifetime $\tau_{eff}$ as a function of $\Delta n$ assuming three different defect configurations. Case 1 represents a defect with the same effective low level injection (LLI) lifetime as the BO defect but a much weaker injection-dependence, case 2 a defect with a significantly higher LLI lifetime than case 1 which roughly represents no BO defect of the BO defect being in an ideal annealed/regenerated state (Cz cell B/ FZ cell) and case 3 the BO defect being in its active state (Cz cell A). For modelling, the assumed defect configurations in the SRH term are (case 1) a mid-gap defect with symmetric capture cross sections and thus equal electron and hole capture time constants of $\tau_{n0}=\tau_{p0}=45$ µs, (case 2) a similar mid-gap defect with reduced defect concentration and thus increased $\tau_{n0}=\tau_{p0}=500$ µs and (case 3) the Cz-specific BO defect with a deep energy level at $E_c-E_t=0.41$ eV and a stronger injection-dependence due to the capture asymmetry with $\tau_{p0}/\tau_{n0}=9.5$ [25]. For the BO defect $\tau_{n0}=44$ µs is assumed. This is in accordance with the parameterisation of the effective lifetime at an injection level of $\Delta n=0.1p_0$ given in [26], with the doping density $N_A=[B_s]=6.23\times10^{15}$ cm$^{-3}$ (according to $p_b=2.3\,\Omega$ cm for the Cz wafers used) and a typical interstitial oxygen concentration of $[O_i]=7.5\times10^{17}$ cm$^{-3}$. For our calculations, we used the parameterisation of the entire SRH term given in [27] which is based on [25,26]. We assume $m=2$ for the process-dependent parameter, which gives $\tau_{BO}(\Delta n=0.1p_0)=$ 84.5 µs, and to calculate the resulting $J$ and $J_{rec}$, a wafer thickness of $W=200$ µm.

Fig. 2a shows, that for $\Delta n\le10^{14}$ cm$^{-3}$, cases 1 and 3 result in comparable effective lifetimes while for $\Delta n>10^{14}$ cm$^{-3}$, the strong injection-dependence of the BO defect leads to an increase in lifetime for case 3. Case 2 exhibits a higher lifetime across the entire relevant excess carrier density range. For $\Delta n>2\times10^{16}$ cm$^{-3}$, $\tau_{eff}$ is dominated by Auger recombination. Calculating a $J$–$V$ curve for the three cases according to Eq. (3) (assuming $J_{ph}=0$ mA/cm$^2$) leads to the curves depicted in Fig. 2b. Since we apply a zero-dimensional model neglecting series resistance $R_s$, the superposition principle [28,29] is valid. That is, the dark $J$–$V$ curve equals the suns–$V_{oc}$ curve and by adding a value of $J_{ph}>0$ mA/cm$^2$, an illuminated $J$–$V$ curve can be derived. Also, the correlation $J(V=0\,V)=J_{sc}=J_{ph}$ holds which is independent of $\Delta n$. In a real device, this is of course not the case for effective lifetimes as given in Fig. 2a. To consider the effect of differing LLI lifetimes between cases 1/3 and case 2 on $J_{sc}$, we assume $J_{sc,case\,1}=J_{sc,case\,3}=38.40$ mA/cm$^2$ and $J_{sc,case\,2}=38.75$ mA/cm$^2$, which reflect the measured degraded and annealed values of the considered Cz solar cells, respectively. Fig. 2d depicts the resulting illuminated $J$–$V$ curves for all three cases. The differences in $V_{oc}$ are due to the different effective lifetimes at the operation point of open-circuit (OC), as indicated by the vertical lines in Fig. 2a. Due to the increase of the effective lifetime in case 3 compared to case 1 for $\Delta n>10^{14}$ cm$^{-3}$, a higher excess carrier density is reached at OC and therefore a higher $V_{oc}$. All relevant values are given in Table 1.

The maximum power point (MPP) of the curves given in Fig. 2d can be determined and results in a $V_{MPP}$, which can be converted into a corresponding $\tau_{eff,MPP}/\Delta n_{MPP}$ pair according to Eqs. (1) and (2). Figs. 2a and c indicate the results. Since the effective lifetimes at the MPP in cases 1 and 3 are almost identical, the values of $V_{MPP}$ are very similar. Since $J_{sc,case\,1}=J_{sc,case\,3}$ is assumed due to equal LLI lifetimes, almost identical values for $J_{MPP}$ and therefore for the efficiencies $\eta$ result, as can be seen in Table 1. For case 2, higher values of $V_{MPP}$ and $\eta$ result due to the significantly higher effective lifetime and therefore excess carrier density at the MPP. When comparing cases 1 and 3, $J_{sc}$ is equal, $\eta$ is almost equal and $V_{oc}$ significantly differs. As the fill factor is defined via $FF=(J_{MPP}\times V_{MPP})/(J_{sc}\times V_{oc})$, case 1 results in a significantly higher

**Table 1**
Short-circuit current density $J_{sc}$, voltage $V$, excess carrier density $\Delta n(V)$ and effective lifetime $\tau_{eff}(\Delta n(V))$ at the maximum power point (index MPP) and under open-circuit conditions (index OC) as well as fill factor $FF$ and efficiency $\eta$ resulting from a zero-dimensional model (simulation parameters are given in Section 3). Case 1 represents a defect with $\tau_{n0}=\tau_{p0}=45\,\mu s$ and $E_t=E_i$, case 2 with $\tau_{n0}=\tau_{p0}=500\,\mu s$ and $E_t=E_i$ and case 3 the BO defect being in its active state according to [27] with $m=2$, $[B_s]=6.23\times10^{15}\,cm^{-3}$ and $[O_i]=7.5\times10^{17}\,cm^{-3}$ based on [25,26].

| Case | $J_{sc}$ (mA/cm$^2$) | $V_{MPP}$ (mV) | $\Delta n(V_{MPP})$ (cm$^{-3}$) | $\tau_{eff}(\Delta n(V_{MPP}))$ (μs) | $V_{oc}$ (mV) | $\Delta n(V_{oc})$ (cm$^{-3}$) | $\tau_{eff}(\Delta n(V_{oc}))$ (μs) | $FF$ (%) | $\eta$ (%) |
|---|---|---|---|---|---|---|---|---|---|
| 1 | 38.40 | 543 | $2.41\times10^{13}$ | 45.0 | 627 | $5.82\times10^{14}$ | 48.6 | 82.7 | 19.9 |
| 2 | 38.75 | 605 | $2.60\times10^{14}$ | 499.6 | 710 | $7.37\times10^{15}$ | 606.2 | 81.6 | 22.4 |
| 3 | 38.40 | 545 | $2.61\times10^{13}$ | 46.1 | 656 | $1.57\times10^{15}$ | 131.2 | 79.2 | 19.9 |

$FF$ than case 3 with $FF_{case\ 1}-FF_{case\ 3}=3.5\%_{abs}$. Since in case 3, which reflects the BO defect in its active state, the significant increase in effective lifetime with $\Delta n$ occurs after the MPP, $\eta$ cannot benefit from this increase but $V_{oc}$ is superelevated compared to the conditions at MPP. Hence, a solar cell being represented by case 3 does not exhibit a classical "fill factor problem" with possible root causes of increased series resistance $R_s$ or decreased parallel resistance $R_p$ but the fill factor is solely limited due to the intrinsic injection-dependence of the SRH lifetime of the BO defect in its active state. Since this effect is not linked to $R_s$, it also shows in the pseudo-fill factor $pFF$ of real solar cells as will be shown later. In-between MPP and OC point, the $J_{rec}$–$V$ (respectively suns–$V_{oc}$) curve of case 3 exhibits a strong kink compared to case 1. Case 2 also shows a less pronounced kink which results in a lower $FF$ than case 1, see Table 1. As stated above, the given $FF$s equal the respective $pFF$s and $\eta$ equals the respective pseudo-efficiency $p\eta$.

## 4. Characterisation

### 4.1. Solar cell level

In the following section, the experimental results up to the module integration step are discussed. First, the impact of activation, deactivation and regeneration of the BO defect on illuminated $I$–$V$ parameters is addressed. Second, the impact on fill factor $FF$ is investigated in more detail.

#### 4.1.1. Illuminated I–V parameters

Fig. 3a depicts the illuminated $I$–$V$ curve of Cz cell B in the annealed, degraded and regenerated state. Qualitatively, the curves follow the behaviour of the curves for cases 2 (ann./reg.) and 3 (deg.) shown in Fig. 2d. As can be seen, the activation of the BO defect by illumination degrades $I_{sc}$, $V_{oc}$ and $FF$ which, each,can be recovered by regeneration. Since the degradation of $I_{sc}$ is used as an input parameter in Section 3 for the zero-dimensional model, Fig. 3b depicts the internal quantum efficiency $IQE$ of Cz cell B in the degraded and regenerated state. Both curves only differ in the wavelength range from $\lambda\approx750$ nm to 1150 nm which is affected by bulk lifetime [30,31]. This shows that the difference in $I_{sc}$ between defect states can be attributed to material-induced bulk effects.

Fig. 4a shows the measurement results of the illuminated $I$–$V$ parameters $V_{oc}$, short-circuit current $I_{sc}$, $FF$, $pFF$, ideal fill factor $FF_0$ and maximum output power $P_{MPP}$ after each step as sketched in Fig. 1. Due to the higher base doping, the FZ reference cell exhibits a slightly lower $I_{sc}$ and a higher $V_{oc}$ compared to the Cz cells in the annealed state.

To highlight the impact of annealing (ANN), degradation (DEG) and regeneration (REG) on the different cell parameters, Fig. 4b depicts for each of the three cells the absolute differences compared to the values in the degraded state. Comparing for example the annealed with the degraded state, a significant reduction of the output power is observed for both Cz cells which amounts to $\Delta P_{MPP,Cz\ A}=-0.13$ W and $\Delta P_{MPP,Cz\ B}=-0.12$ W. The output power can be directly converted into efficiencies which are for Cz cell A $\eta_{Cz\ A,\ ANN}=19.1\%$ ($P_{MPP,Cz\ A,\ ANN}=2.84$ W) in the annealed state and $\eta_{Cz\ A,\ DEG}=18.2\%$ ($P_{MPP,Cz\ A,\ DEG}=2.71$ W) in the degraded state. Hence, the observed loss in output power of $\Delta P_{MPP,Cz\ A}=-0.13$ W corresponds to a loss in efficiency of $\Delta\eta_{Cz\ A}=-0.9\%_{abs}$. Any further given power values on cell level can be converted into efficiencies accordingly. Comparing the annealed and the degraded state for the FZ cell, it can be seen that – as expected – the FZ cell is stable in all parameters.

The degradation-induced loss in the output power of the Cz cells originates from a decrease in all three cell parameters: $V_{oc}$, $I_{sc}$ and $FF$. The voltage losses of $\Delta V_{oc,Cz\,A}=-10.6$ mV and $\Delta V_{oc,Cz\,B}=-8.8$ mV and current losses of $\Delta I_{sc,Cz\,A}=\Delta I_{sc,Cz\,B}=-0.05$ A are caused by the reduction of the bulk lifetime due to the activation of the BO complex, see Section 3 and Fig. 3b. The fill factor losses of $\Delta FF_{Cz\ A}=-1.6\%_{abs}$ and $\Delta FF_{Cz\ B}=-1.5\%_{abs}$ predominantly result from losses in pseudo-fill factor ($pFF$). This $FF$ loss will be discussed in more detail in Section 4.1.2.

The degradation-induced losses in the Cz cells can be recovered by regeneration while the FZ reference cell is stable in all three states. As can be seen in Fig. 4, this recovery is stable upon a second degradation cycle which is performed under the same conditions as the previous degradation but for a longer time of five days. This forth state is thus called "stabilized". Hence, as expected from literature, the recombination-active defect centre related to the BO complex seems to be permanently deactivated by the applied regeneration procedure with simultaneous heating and illumination, at least on solar cell level.

#### 4.1.2. In-depth characterisation of fill factor FF

In order to determine which amount of the observed $FF$ variation in-between defect states is caused by the impact of the BO defect on lifetime, the effects on $FF$ are investigated in detail. A limitation of the $FF$ can be composed of multiple contributions. (i) The trivial cause is, that a lower $V_{oc}$ also leads to a lower $FF$. Applying Green's formula for the maximum fill factor $FF_0$ of an ideal diode with ideality factor $n=1$ (p. 96 in [32]), a drop in $V_{oc}$ of $\Delta V_{oc}=646$ mV − 636 mV = 10 mV, as it is observed for the Cz cells, results in a drop in $FF_0$ of $\Delta FF_0=83.73\%-83.55\%=0.18\%_{abs}$. (ii) A further effect degrading fill factor is series resistance $R_s$. When $R_s$ is assumed to be lumped and/or small, which is the case for the cells discussed here, its effect on the pseudo-fill factor can be neglected [33]. (iii) The $pFF$, however, can be affected by parallel resistance $R_p$ when being too low. The measured values are $R_{p,\ Cz\ A/B}>10\,k\Omega\,cm^2$, $R_{p,\ FZ}>4\,k\Omega\,cm^2$ and, therefore, do not degrade $pFF$ significantly. (iv) Additional losses of the fill factor can originate from non-idealities of the diode such as injection-dependent changes in minority carrier lifetime along the course of the $I$–$V$ curve. This influences the fill factor of the $I$–$V$ curve under 1 sun illumination and the $pFF$ [20,21] in a similar manner, as derived in Section 3. The root causes for

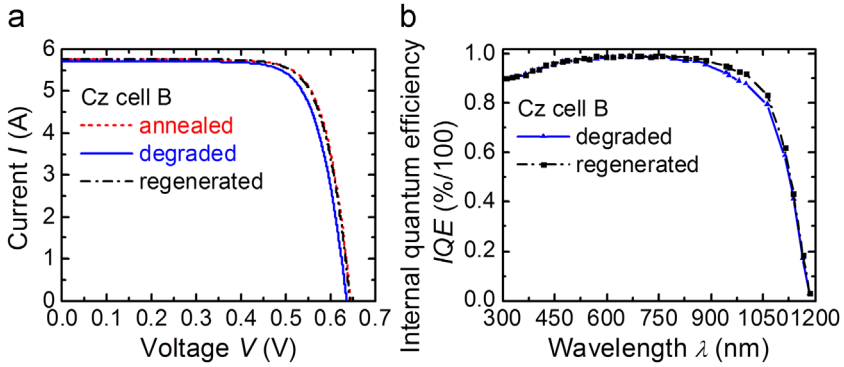


**Fig. 3.** (a) Illuminated *I–V* curves of Cz cell B in the annealed, degraded and regenerated state. (b) Internal quantum efficiency *IQE* as a function of wavelength for the same cell in the degraded and regenerated state.

injection-dependent lifetime include recombination in the space charge region, injection-dependent bulk lifetime (see Section 3) and injection-dependent surface recombination velocity.

We quantify the fill factor differences due to the activation and deactivation of the BO defect by using a fill factor loss analysis according to [33] with an emphasis on the *pFF*. To motivate this approach, we discuss the suns–$V_{oc}$ curves of all three cells for the three discussed defect states in the following paragraphs.

If the non-idealities of a solar cell are described with a voltage-dependent saturation current density $J_0(V)$ rather than with a second diode [2,3] and/or a voltage-dependent local ideality factor [34], a solar cell's suns–$V_{oc}$ characteristic can be written as

$$cE(V_{oc}) = J_0(V_{oc})\left(\exp\left(\frac{V_{oc}}{V_t}\right)-1\right), \tag{4}$$

with the constant $c$ being the conversion factor between $E$ and $J$. We assume $R_p$ being sufficiently high to not affect the characteristic which is the case for the discussed cells (see above). The proportionality of illumination intensity $E$ and $J_{sc}$ has been confirmed on Cz and FZ cells from the same batch by measurements in the intensity range of $E=0.1$–$1.2$ suns. If we consider two defect states of the same cell, for example the annealed and the degraded state,

$$cE = J_0(V_{oc,ANN})\left(\exp\left(\frac{V_{oc,ANN}}{V_t}\right)-1\right) = J_0(V_{oc,DEG})\left(\exp\left(\frac{V_{oc,\ DEG}}{V_t}\right)-1\right) \tag{5}$$

holds true for every illumination intensity $E$. Assuming $\exp(V_{oc}/V_t) \gg 1$, an open-circuit voltage difference of

$$\Delta V_{oc} = V_{oc,ANN} - V_{oc,DEG} = V_t \ln\left(\frac{J_0(V_{oc,DEG})}{J_0(V_{oc,ANN})}\right) \tag{6}$$

can be calculated which does not directly depend on $E$. However, $V_{oc,DEG}$ and $V_{oc,ANN}$ are both functions of $E$. Hence, if $J_0$ shows a different injection-dependence in different defect states of the same cell, $\Delta V_{oc}$ will vary with illumination intensity $E$. The stronger $\Delta V_{oc}$ varies with varying $E$, the stronger is the difference in the injection-dependence of $J_0$ in-between the two states.

Fig. 5a (top) depicts the suns–$V_{oc}$ curves of Cz cell A in the annealed and degraded state. The kink in the degraded curve is not as pronounced as in Fig. 2c but still prominent. When comparing $\Delta V_{oc}(E=0.05$ suns), which is close to the maximum power point of the $J_{sc}$-shifted suns–$V_{oc}$ curve (pMPP), and $\Delta V_{oc}(E=1.0$ suns), a decrease of $\Delta V_{oc}$ from $\Delta V_{oc}(E=0.05$ suns$)=17.2$ mV to $\Delta V_{oc}$ $(E=1.0$ suns$)=10.6$ mV with increasing illumination intensity $E$ can be observed, as shown in Fig. 5b. This results in a drop in *pFF* of $\Delta pFF = -1.2\%_{abs}$. The ideal fill factor $FF_0$ drops by $\Delta FF_0 = -0.2\%_{abs}$ due to $\Delta V_{oc}(E=1.0$ sun$)=10.6$ mV, compare contribution (i) discussed above. Hence, it can be concluded that the remaining pseudo-fill factor loss of $\Delta pFF = -1.0\%_{abs}$ is caused by the changes in injection-dependent SRH lifetime upon activation of the BO defect.

Fig. 5 and Table A1 (see Appendix) also show the respective plots and values for Cz cell B and the FZ reference cell considering the annealed, degraded and regenerated state. The voltage difference $\Delta V_{oc}$ between annealed and degraded state behaves similarly for Cz cells A and B causing a similar effect on *pFF*. For the FZ cell, the annealed and degraded curves line up very closely exhibiting values of $\Delta V_{oc} < 2$ mV across the considered illumination intensity range causing no degradation in *pFF*. When considering $\Delta V_{oc}$ between the annealed and regenerated state, an increase towards lower illumination intensities occurs for Cz cell B and the FZ reference cell. This increase is in the same order for both cells which indicates, that the effect is process- and not material-induced. However, this effect only accounts for a loss in *pFF* of $\Delta pFF \geq -0.3\%_{abs}$ compared to the discussed $\Delta pFF = -1.0\%_{abs}$ which results from only the changes in injection-dependent lifetime upon activation of the BO defect. This *pFF* difference is in good agreement with values found by Schmidt et al. [20,35].

Fig. 4 summarises the results of the fill factor analysis (additional values are given in Table A1). The fill factor degradation from the annealed to the degraded state for the Cz cells is mainly caused by a degradation in *pFF* due to the strong injection-dependence of the SRH lifetime of the activated BO complex, as discussed in Section 3. By regeneration, the original fill factor value can almost be recovered and is stable upon subsequent illumination for five days. As this behaviour is characteristic to the metastable BO defect, we exclude other injection-dependent mechanisms, such as injection-dependent surface recombination velocity, as causes for the fill factor degradation. The *FF* of the FZ cell does not change to a large extent in-between all preparation steps conducted on cell level which proofs that there are no major process-induced effects on *FF*.

In summary, characterising the different states on cell level reveals that, for Cz cell B, all illuminated *I–V* parameters ($V_{oc}$, $I_{sc}$ and *FF*) can be almost completely recovered by the regeneration step and are stable upon subsequent illumination for five days while the reference FZ cell does not degrade.

### 4.2. Module level

With the solar cells being conditioned in different states, the next steps in the experimental design, see Fig. 1, are module integration and subsequent illumination to investigate whether the achieved gain by regeneration of the boron–oxygen defect on

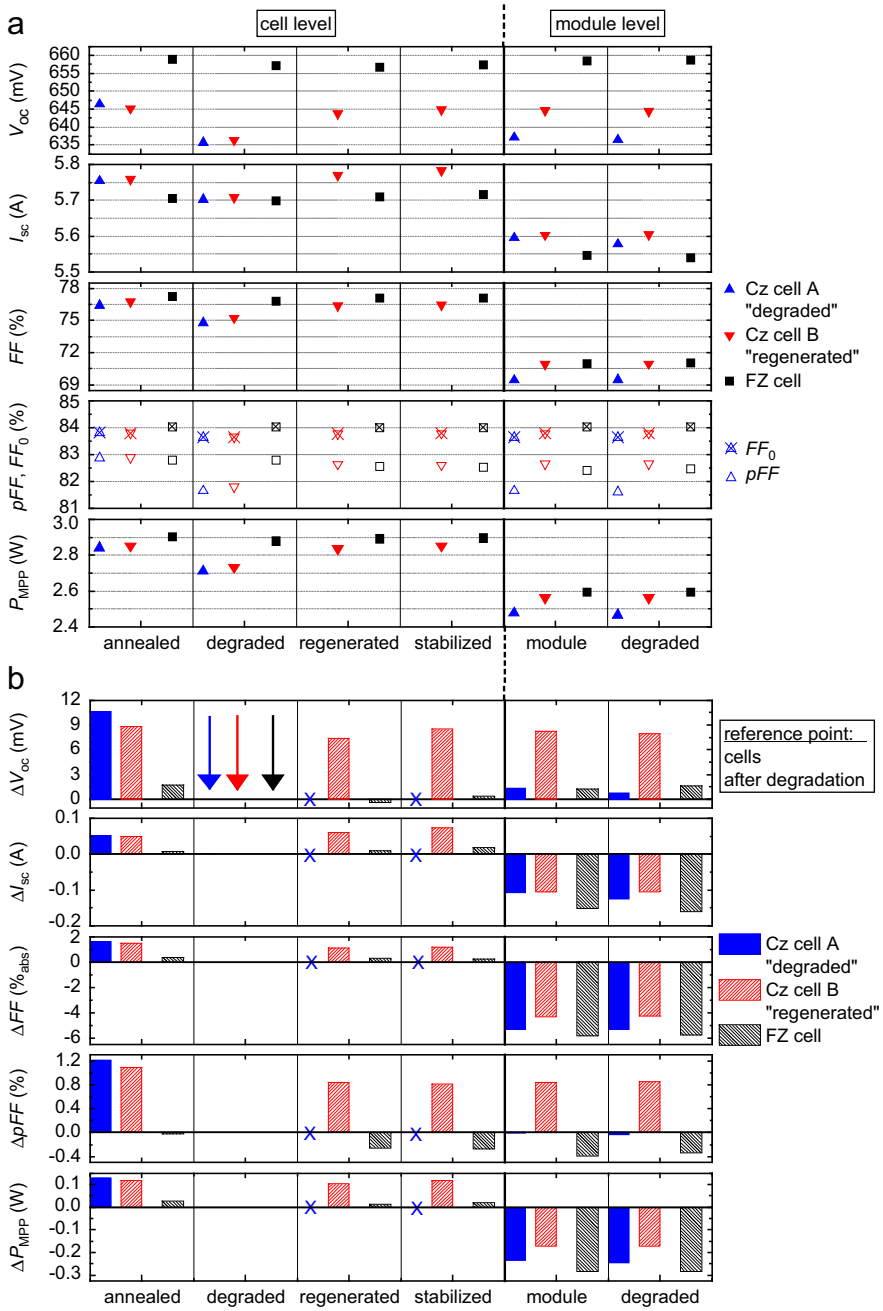


**Fig. 4.** (a) Measured illuminated *I–V* parameters open-circuit voltage $V_{oc}$, short-circuit current $I_{sc}$, fill factor *FF*, pseudo-fill factor *pFF*, ideal fill factor $FF_0$ and maximum output power $P_{MPP}$ after each conditioning step sketched in Fig. 1. (b) Absolute differences in the different conditioning steps compared to values after degradation (indicated by arrows) for each of the three cells.

cell level is transferable to module level. For the *I–V* and suns–$V_{oc}$ measurements on module level, different shading patterns have been applied to control the effect of total internal reflection under the module glass. All given measurement values have been recorded with a shading pattern representing the symmetry element in a standard industrial module, that is a square pattern with an opening of $A = 127 \times 127\ mm^2$ simulating the distance of cells in a module to be $d = 2$ mm.

To interpret the results, Figs. 4 and 6 have to be considered coherently. Fig. 6 shows the differences in $V_{oc}$, $I_{sc}$, *FF*, *pFF* and $P_{MPP}$ compared to the values of each cell in a reference state before module integration. That is, for Cz cell A the degraded state, for Cz cell B the stabilized state after successful regeneration and for the FZ cell the state after the same treatment as for Cz cell B.

The deviation in $V_{oc}$ before and after module integration is $\Delta V_{oc} < 1.5$ mV for all cells which shows that there is no significant degradation. As illustrated in Fig. 4b, the gain in $V_{oc}$ of $\Delta V_{oc} \approx 8$ mV due to regeneration of the BO defect compared to the degraded values can be transferred to module level. This is also true after subsequent illumination of the modules for $t > 48$ h. For a rough, theoretical estimate of possible temperature-induced effects during the moduling process on $V_{oc}$, Herguth's [10] data on the temperature-dependent decay constants on cell level for the destabilization of the regenerated state in the dark are used. However, the experimental data provided by Herguth are not in the range of the applied temperatures during the moduling process. Hence, his data need to be extrapolated to higher and lower temperatures. For $V_{oc}$, Herguth determined the activation

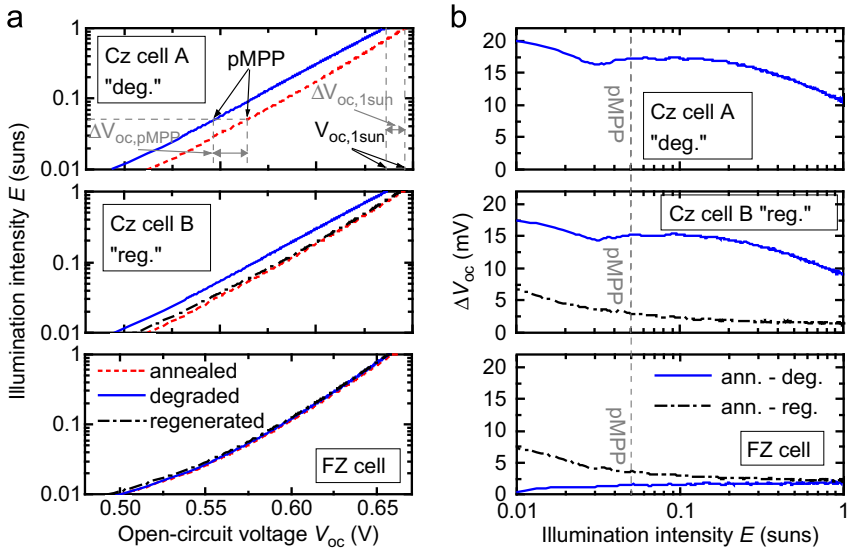


**Fig. 5.** (a) Measured suns–$V_{oc}$ curves of all three considered cells for the three different defect states. (b) Difference in open-circuit voltages $V_{oc}$ in-between different defect states for the three cells as a function of illumination intensity $E$.

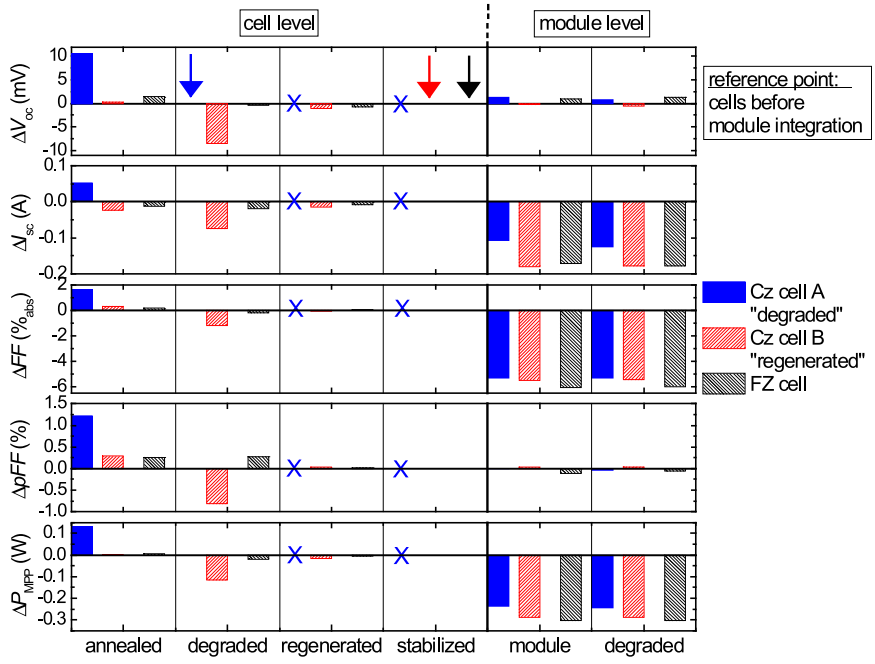


**Fig. 6.** Absolute difference in open-circuit voltage $V_{oc}$, short-circuit current $I_{sc}$, fill factor $FF$, pseudo-fill factor $pFF$ and maximum output power $P_{MPP}$ compared to values of each cell before module integration (indicated by arrows). Note, that Fig. 6 shows the same data as Fig. 4b but calculated with respect to a different reference point for each cell.

energy of the destabilization to be $E_a \approx 1$ eV. By manually parameterising and extrapolating Herguth's Arrhenius plot from [10], decay constants of $c_{decay}(T_{soldering}=225\ ^\circ C)=1.1\times10^{-1}\ min^{-1}$ and $c_{decay}(T_{lamination}=133\ ^\circ C)=7.2\times10^{-4}\ min^{-1}$ result. Assuming worst case conditions for the applied moduling process (see Section 2), that is $t(T=225\ ^\circ C)=2$ s and $t(T=133\ ^\circ C)=30$ min, a loss of less than $3\%_{rel}$ in $V_{oc}$ gain is calculated. Although in general extrapolated data need to be considered with care, our experimental data support Herguth's findings.

Considering $FF$, both Cz cells exhibit the same degradation due to the module integration, as shown in Fig. 6. As the $pFF$ is preserved during module integration, the loss in $FF$ can be fully attributed to additional series resistance losses in the cell interconnectors and feed lines. Due to the layout of the mini-module, the additional series resistance per cell is slightly higher than for standard industrial modules with $n \geq 60$ cells. Fig. 4b illustrates, that the gain in $FF$ and $pFF$ due to regeneration can be transferred to module level and is stable upon subsequent illumination of the module.

Concerning $I_{sc}$, Fig. 4b shows that the $I_{sc}$ advantage due to regeneration of the BO defect can be transferred to module level when comparing Cz cell B to the FZ reference. However, compared to Cz cell A, which is in the degraded state before module integration, the gain in $I_{sc}$ due to regeneration on cell level cannot be completely transferred to module level, as can be seen in Fig. 4b. The effect of differing $I_{sc}$ losses in-between modules

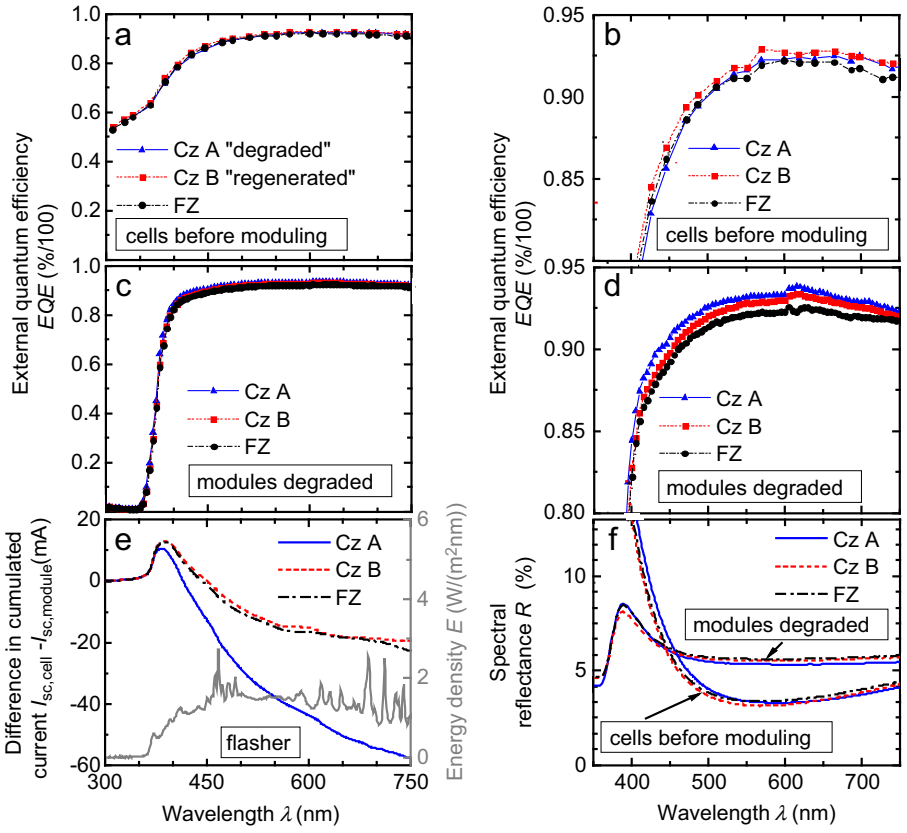


**Fig. 7.** (a) Measured external quantum efficiency *EQE* of the three discussed cells before module integration. (b) Cut-out of Fig. 7a. (c) *EQE* of the cells when being encapsulated. (d) Cut-out of Fig. 7c. (e) Difference in cumulated $I_{sc}$ values between cell and module level calculated according to Eq. (7) using the measured spectrum of the applied flasher during *I–V* testing. (f) Spectral reflectance before and after module integration.

becomes more pronounced when considering the absolute difference of $I_{sc}$ compared to its values before module integration (see Fig. 6). Cz cell B and the FZ cell lose $\Delta I_{sc,moduling} = -179$ mA and $-178$ mA, respectively, due to module encapsulation while Cz cell A, surprisingly, only loses $\Delta I_{sc,moduling} = -125$ mA. The difference in $I_{sc}$ degradation upon module encapsulation between Cz cell A and B amounts to $\Delta I_{sc,moduling,\ Cz\,A} - \Delta I_{sc,moduling,\ Cz\,B} = -125\ \text{mA} - (-179\ \text{mA}) = 54$ mA. Both, $V_{oc}$ and *pFF*, remain constant during module assembly, which indicates that Cz cell A is still in its degraded state. There are three main effects that could cause different absolute losses in $I_{sc}$ during moduling: (i) differences in optical coupling of the individual cells when comparing air and module encapsulation, (ii) different parasitic absorption of the glass and EVA of the different modules, and (iii) different effective shading caused by the soldered cell interconnectors. Different shading and backsheet scattering due to different alignments of the shading pattern during *I–V* measurements can be excluded as repeated measurements show.

All three effects should influence the external quantum efficiencies (*EQE*) of the considered cells and modules. As shown in Fig. 3, the effect of activation and deactivation of the BO defect affects quantum efficiency for wavelengths of $\lambda > 750$ nm. To focus on the effects related to the moduling process only, wavelengths up to $\lambda = 750$ nm are considered in the following discussion. Fig. 7a depicts the measured *EQE* of the three considered cells in their state before module encapsulation and Fig. 7b a cut-out. It can be seen that, in the depicted wavelength range, the *EQE* of Cz cells A (being degraded) and B (being regenerated) are almost identical. Fig. 7c depicts the *EQE* of the three cells after module encapsulation and Fig. 7d a cut-out. It can be seen that the module encapsulation is non-transparent for wavelengths $\lambda < 355$ nm. To estimate the effect of differing *EQE* on cell and module level on $I_{sc}$, we calculate a cumulated $I_{sc,cumulated}$ giving the integrated spectral contribution up to a wavelength $\lambda$ via

$$I_{sc,cumulated}(\lambda) = \int_{\lambda\,=\,300\ \text{nm}}^{\lambda} S(\lambda')EQE(\lambda')\frac{q\lambda'}{hc}\,d\lambda', \tag{7}$$

with $S(\lambda)$ being the energy density of the irradiated spectrum, $h$ Planck's constant and $c$ the speed of light. Fig. 7e shows the difference in $I_{sc,cumulated}$ between cell and module level for each cell using the measured spectrum of the flasher used for *I–V* measurements within the industrial cell tester at Fraunhofer ISE, see right hand axis in Fig. 7e. The cumulated cell-to-module $I_{sc}$ difference exhibits a maximum at $\lambda \approx 385$ nm due to the parasitic absorption in the module encapsulation. For higher wavelengths, the difference decreases; this decrease in $\Delta I_{sc,cumulated}$ is more pronounced for Cz cell A than for the other two cells. Up to $\lambda = 750$ nm, this accounts for $\Delta I_{sc}(\lambda = 750\ \text{nm}) \approx 35$–$38$ mA. When using the AM1.5G spectrum [36] to calculate $I_{sc,cumulated}$, a difference of $\Delta I_{sc}(\lambda = 750\ \text{nm}) \approx 35$–$39$ mA results which is almost identical to the values resulting from using the measured flasher spectrum. This indicates a good quality of the applied flash lamp. Hence, calculating a cumulated cell-to-module $I_{sc}$ difference up to $\lambda = 750$ nm explains almost three quarters of the measured difference in $I_{sc}$

The parasitic absorption of the module encapsulation system leads to a maximum in $\Delta I_{sc,cumulated}$ at $\lambda \approx 385$ nm, see Fig. 7e. The absolute magnitude of the maximum of Cz cell A compared to the other two cells is slightly lower but only accounts for $\Delta I_{sc} \approx 3$–$4$ mA which shows that differences in the parasitic absorption of the module encapsulation system are unlikely as the root cause for the current difference. When comparing the spectral reflectance of the entire encapsulated cell with the spectral reflectance

of a position in-between busbars of the cells, the additional shading contribution of the cell interconnectors can be assessed. Since this parameter does not differ significantly in-between the three cells, also parasitic shading due to cell interconnectors is implausible as the root cause. That leaves differences in optical coupling due to slightly differing indices of refraction, thicknesses of the anti-reflective coating and/or differing back-reflection from the glass due to differing metallisation finger shapes as remaining, possible explanations. This thesis is also supported by a slight difference in the measured spectral reflectance of the three cells on cell and module level, see Fig. 7f. This is also visible in the *EQE* in Figs. 7b and d. The last quarter of the observed deviation is suspected to originate from better optical coupling in the wavelength range of 750 nm $< \lambda <$ 1200 nm.

In summary, the relative gain in $V_{oc}$ and *FF* due to regeneration can be transferred to module level while the module encapsulation-induced loss in $I_{sc}$ is slightly smaller for Cz cell A compared to the other two cells. However, a significant gain in $P_{MPP}$ can still be transferred to module level, as can be seen in Fig. 4a. The difference between Cz cell B (being regenerated) and Cz cell A (being degraded) before module integration amounts to $\Delta P_{MPP}=139$ mW. On module level, the difference between both cells still amounts to $\Delta P_{MPP}=96$ mW. Comparing Cz cell B with the FZ cell in the same manner, values of $\Delta P_{MPP}=-49$ mW before and $\Delta P_{MPP}=-32$ mW after module integration result. Hence, it can be concluded, that a gain due to regeneration of the BO defect on cell level can be transferred to module level.

## 5. Summary and conclusion

Regenerating the BO defect in passivated emitter and rear solar cells fabricated on industrial boron-doped *p*-type Cz wafers with a base resistivity of $\rho_b=2.3\ \Omega$ cm leads to an increase in all illuminated *I–V* parameters resulting in an efficiency gain of $\Delta\eta_{cell}=0.8$–$0.9\%_{abs}$. In accordance with previous studies, it is shown that the difference in *FF* is mainly due to the injection-dependent SRH lifetime of the BO defect in its active state accounting for a regeneration-induced fill factor gain of $\Delta FF_{cell} > 1.0\%_{abs}$. This effect also shows in the *pFF* which can be determined from suns–$V_{oc}$ measurements. The experimentally observed effects can be described qualitatively by simulating the impact of activation and deactivation of the BO defect on solar cell parameters.

We have shown that the benefit achieved by regeneration on solar cell level can be transferred to module level when applying industrially used processing steps such as soldering and lamination, and is stable upon subsequent illumination. The *I–V* parameters of Cz cell B (which is in the regenerated state before moduling) suffer from the same amount of module encapsulation-induced losses as the FZ reference cell. Hence, no Cz-specific degradation of the "regenerated" Cz cell B during module encapsulation is observed. Except for short-circuit current, the same effect is observed for Cz cell A which is in the degraded state before moduling. The difference in $I_{sc}$ in-between Cz cell A and B on module level is most likely due to differences in optical coupling.

These results indicate, that regeneration of the BO defect on cell level might be a possible solution to overcome efficiency limitations of solar cells and modules fabricated from boron-doped *p*-type Cz silicon wafers.

## Acknowledgements

The authors would like to acknowledge Ulrich Jäger for allocation of the investigated solar cells, Elisabeth Schäffer for QE measurements, Marco Tranitz for module manufacturing and Alexander Krieg for *I–V* measurements and calibration of the cell tester. Part of this work was supported by the German Federal Ministry of Environment, Nature Conservation and Nuclear Safety under Contract no. 0329849B.

## Appendix A

See Table A1.

**Table A1**
Differences in ideal fill factor $FF_0$, pseudo-fill factor *pFF*, fill factor *FF* and open-circuit voltages $V_{oc}$ for illumination intensities of $E=0.05$ suns (representing the pMPP) and $E=1.0$ suns, in relation to the annealed state for all three considered cells.

| State | Difference to annealed state | Cz cell A ("degraded") | Cz cell B ("regenerated") | FZ reference |
|---|---|---|---|---|
| Degraded | $\Delta FF_0$ | $-0.2\%_{abs}$ | $-0.1\%_{abs}$ | $0.0\%_{abs}$ |
| | $\Delta pFF$ | $-1.2\%_{abs}$ | $-1.1\%_{abs}$ | $0.0\%_{abs}$ |
| | $\Delta FF$ | $-1.6\%_{abs}$ | $-1.5\%_{abs}$ | $-0.4\%_{abs}$ |
| | $\Delta V_{oc}(E=0.05$ sun) | −17.2 mV | −15.2 mV | −1.6 mV |
| | $\Delta V_{oc}(E=1.0$ sun) | −10.6 mV | −8.8 mV | −1.8 mV |
| Regenerated | $\Delta FF_0$ | – | $0.0\%_{abs}$ | $0.0\%_{abs}$ |
| | $\Delta pFF$ | – | $-0.3\%_{abs}$ | $-0.2\%_{abs}$ |
| | $\Delta FF$ | – | $-0.4\%_{abs}$ | $-0.1\%_{abs}$ |
| | $\Delta V_{oc}(E=0.05$ sun) | – | −2.9 mV | −3.6 mV |
| | $\Delta V_{oc}(E=1.0$ sun) | – | −1.5 mV | −2.2 mV |
| Stabilized | $\Delta FF_0$ | – | $0.0\%_{abs}$ | $0.0\%_{abs}$ |
| | $\Delta pFF$ | – | $-0.3\%_{abs}$ | $-0.3\%_{abs}$ |
| | $\Delta FF$ | – | $-0.3\%_{abs}$ | $-0.2\%_{abs}$ |
| | $\Delta V_{oc}(E=0.05$ sun) | – | −3.2 mV | −3.3 mV |
| | $\Delta V_{oc}(E=1.0$ sun) | – | −0.3 mV | −1.4 mV |
| Module | $\Delta FF_0$ | $-0.2\%_{abs}$ | $0.0\%_{abs}$ | $0.0\%_{abs}$ |
| | $\Delta pFF$ | $-1.2\%_{abs}$ | $-0.3\%_{abs}$ | $-0.4\%_{abs}$ |
| | $\Delta FF$ | $-6.9\%_{abs}$ | $-5.8\%_{abs}$ | $-6.2\%_{abs}$ |
| | $\Delta V_{oc}(E=0.05$ sun) | −16.4 mV | −2.3 mV | −3.4 mV |
| | $\Delta V_{oc}(E=1.0$ sun) | −9.3 mV | −0.6 mV | −0.5 mV |
| Module, degraded | $\Delta FF_0$ | $-0.2\%_{abs}$ | $0.0\%_{abs}$ | $0.0\%_{abs}$ |
| | $\Delta pFF$ | $-1.2\%_{abs}$ | $-0.2\%_{abs}$ | $-0.3\%_{abs}$ |
| | $\Delta FF$ | $-6.9\%_{abs}$ | $-5.8\%_{abs}$ | $-6.2\%_{abs}$ |
| | $\Delta V_{oc}(E=0.05$ sun) | −17.2 mV | −2.4 mV | −2.7 mV |
| | $\Delta V_{oc}(E=1.0$ sun) | −9.9 mV | −0.8 mV | −0.1 mV |

## References

[1] W. Zulehner, D. Huber, Crystals Growth, Properties and Applications, vol. 8, Springer Verlag, Berlin Heidelberg, 1982.
[2] A. Goetzberger, B. Voß, J. Knobloch, Sonnenenergie: Photovoltaik, Teubner Studienbücher Physik, Stuttgart, 1994.
[3] A. Goetzberger, J. Knobloch, B. Voss, Crystalline Silicon Solar Cells, John Wiley & Sons Ltd., Chichester, UK, 1998.
[4] J. Schmidt, K. Bothe, Structure and transformation of the metastable boron- and oxygen-related defect center in crystalline silicon, Physical Review B: Condensed Matter 69 (2004) 0241071–0241078.
[5] V.V. Voronkov, R. Falster, Latent complexes of interstitial boron and oxygen dimers as a reason for degradation of silicon-based solar cells, Journal of Applied Physics 107 (2010) 1–8.
[6] S. Rein, W. Warta, S.W. Glunz, Investigation of carrier lifetime in *p*-type Cz-silicon: specific limitations and realistic prediction of cell performance, in: Proceedings of the 28th IEEE Photovoltaics Specialists Conference, Anchorage, Alaska, USA, 2000, pp. 57–60.
[7] J. Schmidt, B. Lim, D. Walter, K. Bother, S. Gatz, T. Dullweber, P.P. Altermatt, Impurity-related limitations of next-generation industrial silicon solar cells, IEEE Journal of Photovoltaics 3 (2013) 114–118.
[8] S.W. Glunz, S. Rein, W. Warta, J. Knobloch, W. Wettling, On the degradation of Cz-silicon solar cells, in: Proceedings of the 2nd World Conference on Photovoltaic Energy Conversion, Vienna, Austria, 1998, pp. 1343–1346.
[9] J. Schmidt, A.G. Aberle, R. Hezel, Investigation of carrier lifetime instabilities in Cz-grown silicon, in: Proceedings of the 26th IEEE Photovoltaic Specialists Conference, Anaheim, California, USA, 1997, pp. 13–18.
[10] A. Herguth, G. Schubert, M. Kaes, G. Hahn, A new approach to prevent the negative impact of the metastable defect in boron doped cz silicon solar cells,

in: Proceedings of the 4th World Conference on Photovoltaic Energy Conversion, Waikoloa, Hawaii, USA, 2006, pp. 940–943.
[11] B. Lim, Boron–Oxygen-Related Recombination Centers in Crystalline Silicon and the Effects of Dopant-Compensation, Ph.D. Thesis, Fakultät für Mathematik und Physik, Universität Hannover, Hannover, 2012.
[12] A. Herguth, G. Hahn, Boron–oxygen related defects in cz-silicon solar cells degradation, regeneration and beyond, in: Proceedings of the 24th European Photovoltaic Solar Energy Conference, Hamburg, Germany, 2009, pp. 974–976.
[13] P. Schmitt, P. Kaiser, C. Savio, M. Tranitz, U. Eitner, Intermetallic phase growth and reliability of Sn–Ag-soldered solar cell joints, Energy Procedia 27 (2012) 664–669.
[14] A.W. Blakers, A. Wang, A.M. Milne, J. Zhao, M.A. Green, 22.8% efficient silicon solar cell, Applied Physics Letters 55 (1989) 1363–1365.
[15] D. Biro, R. Preu, S.W. Glunz, S. Rein, J. Rentsch, G. Emanuel, I. Brucker, T. Faasch, C. Faller, G. Willeke, J. Luther, PV-Tec: photovoltaic technology evaluation center—design and implementation of a production research unit, in: Proceedings of the 21st European Photovoltaic Solar Energy Conference, Dresden, Germany, 2006, pp. 621–624.
[16] A. Wolf, D. Biro, J.-F. Nekarda, S. Stumpp, A. Kimmerle, S. Mack, R. Preu, Comprehensive analytical model for locally contacted rear surface passivated solar cells, Journal of Applied Physics 108 (2010) 1–13.
[17] S. Mack, U. Jäger, G. Kästner, E.A. Wotke, U. Belledin, A. Wolf, R. Preu, D. Biro, Towards 19% efficient industrial PERC devices using simultaneous front emitter and rear surface passivation by thermal oxidation, in: Proceedings of the 35th IEEE Photovoltaic Specialists Conference, Honolulu, Hawaii, USA, 2010, pp. 17–21.
[18] U. Jäger, S. Mack, C. Wufka, A. Wolf, D. Biro, R. Preu, Benefit of selective emitters for *p*-type silicon solar cells with passivated surfaces, IEEE Journal of Photovoltaics 3 (2013) 621–627.
[19] R.A. Sinton, A. Cuevas, A quasi-steady-state open-circuit voltage method for solar cell characterization, in: Proceedings of the 16th European Photovoltaic Solar Energy Conference, Glasgow, UK, 2000, pp. 1152–1155.
[20] J. Schmidt, A. Cuevas, S. Rein, S.W. Glunz, Impact of light-induced recombination centres on the current–voltage characteristic of Czochralski silicon solar cells, Progress in Photovoltaics: Research and Applications 9 (2001) 249–255.
[21] D. Macdonald, A. Cuevas, Reduced fill factors in multicrystalline silicon solar cells due to injection-level dependent bulk recombination lifetimes, Progress in Photovoltaics: Research and Applications 8 (2000) 363–375.
[22] W. Shockley, W.T.J. Read, Statistics of the recombinations of holes and electrons, Physical Review 87 (1952) 835–842.
[23] R.N. Hall, Electron–hole recombination in germanium, Physical Review 87 (1952) 387.
[24] M.J. Kerr, A. Cuevas, General parameterization of Auger recombination in crystalline silicon, Journal of Applied Physics 91 (2002) 2473–2480.
[25] S. Rein, S.W. Glunz, Electronic properties of the metastable defect in boron-doped Czochralski silicon: unambiguous determination by advanced lifetime spectroscopy, Applied Physics Letters 82 (2003) 1054–1056.
[26] K. Bothe, R. Sinton, J. Schmidt, Fundamental boron–oxygen-related carrier lifetime limit in mono- and multi-crystalline silicon, Progress in Photovoltaics: Research and Applications 13 (2005) 287–296.
[27] P.P. Altermatt, Models for numerical device simulations of crystalline silicon solar cells—a review, Journal of Computational Electronics 10 (2011) 314–330.
[28] J. Beier, Untersuchung zur Anwendbarkeit des Superpositionsprinzips bei Silizium-Solarzellen, Ph.D. Thesis, Fakultät für Physik, Universität Freiburg, Freiburg, 1992.
[29] F.A. Lindholm, J.G. Fossum, E.L. Burgess, Application of the superposition principle to solar-cell analysis, IEEE Transaction on Electron Devices 26 (1979) 165–171.
[30] M. Spiegel, B. Fischer, S. Keller, E. Bucher, Separation of bulk diffusion length and back surface recombination velocity by improved IQE-analysis, in: Proceedings of the 28th IEEE Photovoltaics Specialists Conference, Anchorage, USA, 2000, pp. 311–314.
[31] P.A. Basore, Extended spectral analysis of internal quantum efficiency, in: Proceedings of the 23rd IEEE Photovoltaic Specialists Conference, Louisville, Kentucky, USA, 1993, pp. 147–152.
[32] M.A. Green, Solar cells: Operating Principles, Technology and System Applications, UNSW, Kensington, 1986.
[33] J. Greulich, M. Glatthaar, S. Rein, Fill factor analysis of solar cells' current–voltage curves, Progress in Photovoltaics: Research and Applications 18 (2010) 511–515.
[34] K.R. McIntosh, Lumps, Humps and Bumps: Three Detrimental Effects in the Current–Voltage Curve of Silicon Solar Cells, Ph.D. Thesis, Centre for Photovoltaic Engineering, University of New South Wales, Sydney, Australia, 2001.
[35] J. Schmidt, A. Cuevas, S. Rein, S.W. Glunz, Fill factor limitations and non-ideal diode behaviour of Czochralski silicon solar cells due to light-induced recombination centres, in: Proceedings of the 17th European Photovoltaic Solar Energy Conference, Munich, Germany, 2001, pp. 1396–1399.
[36] IEC, Photovoltaic Devices—Part 3: Measurement Principles for Terrestrial Photovoltaic (PV) Solar Devices with Reference Spectral Irradiance Data, 2nd ed., International Electrotechnical Commission, 2008.